Novel approaches for the in situ study of the sintering of nuclear oxide fuel materials and their surrogates

Nicolas Clavier, Galy Ingrid Nkou Bouala, Jacques Léchelle, Julien Martinez, Nicolas Dacheux, Renaud Podor

Novel approaches for the *in situ* study of the sintering of nuclear oxide fuel materials and their surrogates

N. Clavier [1,*], G. I. Nkou Bouala [1], J. Léchelle [2], J. Martinez [3],
N. Dacheux [1], R. Podor [1]

1. ICSM, UMR 5257 CEA/CNRS/ ENSCM/Univ. Montpellier, Site de Marcoule - Bât. 426, BP 17171, 30207 Bagnols/Cèze cedex, France
2. CEA,DEN,DEC,SESC,LLCC, Site de Cadarache, 13108 St-Paul lez Durance, France
3. CEA,DEN,DTEC,SECA,LFC, Site de Marcoule, BP 17171, 30207 Bagnols/Cèze cedex, France

* Author to whom all correspondence should be addressed:

Dr. Nicolas CLAVIER
ICSM – UMR 5257 CEA/CNRS/ ENSCM/Univ. Montpellier
Site de Marcoule – Bât 426
BP 17171
30207 Bagnols sur Cèze
France

Phone : + 33 4 66 33 92 08
Fax : + 33 4 66 79 76 11

nicolas.clavier@icsm.fr

Abstract

Sintering is one of the key-point of the processing of ceramic materials. It is then of primary interest for the nuclear fuel cycle, in which it constitutes an important step in the fabrication of either UO_2 or $(U,Pu)O_2$ pellets used in current PWR reactors. The sintering of actinides oxides not only drives the final density and microstructure of the fuels, but also several characteristics that can impact significantly their behavior in the reactor. Dedicated tools are then needed to monitor the microstructure of such materials and forecast their evolution. In this frame, this paper presents the new potentialities offered by the use of environmental scanning electron microscope at high temperature (HT-ESEM) for the study of nuclear ceramics sintering.

First, the results obtained from bulk pellets are detailed, either regarding original fundamental data at the grain level (such as grain boundaries and pores motion), or design of dedicated microstructures through the assessment of grain growth kinetics. Acquisition of sintering maps thanks to the combination of HT-ESEM observations and classical dilatometric measurements are also addressed. In a second part, observations undertaken at the 2-grain scale to monitor the first stage of sintering, dedicated to neck elaboration, are presented, and compared to the results currently provided by numerical models.

Keywords

HT-ESEM; Sintering; Nuclear fuel; Actinide oxide

1. Introduction

Sintering is usually defined as the transformation of a powdered compact into a cohesive material during a heat treatment. As the most common way of preparation of ceramics, it is of primary interest in numerous industrial processes. Among them, sintering is particularly relevant in the nuclear fuel cycle, in which it constitutes an important step in the fabrication of either UO_2 or $(U,Pu)O_2$ pellets used in current PWR reactors [1-4]. The sintering of actinides oxides not only drives the final density and microstructure of the fuel pellets (including average grain size and pore distribution), but also several characteristics that can impact significantly their life-cycle in the reactor, such as final O/M ratio [5], or homogeneity of the cationic distribution in the case of mixed oxides [6]. For these reasons, the operating conditions used during the sintering of nuclear fuels are precisely controlled, either in terms of heating temperature, time or atmosphere.

Sintering of UO_2 pellets is generally operated at about 1700°C for several hours (typically 3-10h) under H_2 reductive atmosphere in order to guarantee a final O/M ratio close to 2.00 [7]. Such conditions usually lead to an almost complete densification of the pellet, i.e. to a final density close to the calculated one [8]. However, the presence of a limited amount of closed porosity is required to contain the fission gasses created during the irradiation. Hence, several additives can be initially mixed to the UO_2 powder to reach a final density ranging from 95 to 97% of the calculated density, such as organic pore formers, or U_3O_8 coming from the recycling of scraps [9]. By these means, the final porosity is composed by small pores due to densification defects, and larger ones coming from the introduction of pore formers. Another important microstructural parameter to control is the final grain size. If early LWR pellets generally presented a small grain size of about 2-3 µm, the increase in the burn-up targeted to optimize the uranium resource led to enlarge the average grain size up to 10-20 µm to ensure fission gas retention [7]. Such enhanced grain growth was generally achieved by doping the UO_2 fuel material with small amounts of various oxides (the redox state of the metal differing from +IV) such as Cr_2O_3 [10, 11] or Nb_2O_5 [12, 13].

In comparison with UO_2, the processes designed to fabricate MOx fuels are much more diverse. This variety first arises from the various utilizations of the fuel, either in LWR or Fast Breeder Reactors (FBR) : as instance, the final density targeted for the pellets can range from 85-95% for FBR to values close to UO_2 fuel for PWRs (i.e. 95-97 %) [7]. Also, two kinds of preparation routes can be envisaged for the preparation of the starting powders.

The most commonly, and currently, used is a conventional powder metallurgy process based on the mixture of UO_2 and PuO_2 parent oxides. This can be achieved directly to reach the desired plutonium content in the fuel, or from the preparation of an initial UO_2/PuO_2 mixture which is further blended with UO_2, such as in the MIMAS (Micronized Master Blend) process used in France and Belgium [14]. In both cases, temperatures of about 1700°C are required to densify the pellets and to form the solid solutions. Indeed, the cationic interdiffusion operating during the heat treatment also lead to an homogenization of the mixed oxide [15]. On the other hand, wet chemistry methods were also envisaged in order to prepare homogenous starting powders that could promote the rapid formation of a solid solution, even when diluted in UO_2. As instance, the AUPuC german process was based on the initial co-precipitation of uranium and plutonium as a $(NH_4)_4(U,Pu)O_2(CO_3)_3$ precursor which was further fired in reducing conditions then blended with UO_2 to produce the starting oxide powder [16]. This type of co-conversion route is also one of the most studied options for the fabrication of future nuclear fuels in the framework of Gen-III and Gen-IV reactors. One can particularly cite the oxalic precipitation which has been widely reported, either concerning the preparation of mixed-oxide powders containing plutonium and/or minor actinides [17, 18] and their sintering [19-21]. In this framework, and even if the co-precipitated powders already tested in an industrial context were not associated to a decreased sintering temperature, several authors tend to suggest that densification of actinides dioxides could be operated at significantly lower temperatures when starting from low-temperature precursors [22-24].

For both UOx and MOx fuels, the optimization of fabrication processes was based on numerous studies dedicated to the densification step. This latter can be divided in three different stages, respectively assigned to the formation of necks between the grains, then to the elimination of open and closed pores through grain growth [25, 26]. The initial stage, which occurs at the microscopic scale was most frequently discussed through modeling. In this aim, the system considered was frequently composed by two spherical grains in contact, and treated by several numerical methods such as molecular dynamics as well as discrete or finite elements methods [27, 28]. On this basis, qualitative results describing the general behavior of the system were generally obtained but frequently failed to provide predictive information regarding to the evolution of a real sample.

Conversely, intermediate and final stages of the sintering of nuclear fuels were addressed both through numerical and experimental works. For this latter part, dilatometry was probably the most frequently employed technique, and can be used to determine the optimal conditions in terms of heating time and temperature for the complete densification of

a ceramic sample. It was thus employed to evaluate the impact of several operating parameters, such as atmosphere [8, 29], composition [15, 30] or preparation method on the sintering kinetics [23]. Dilatometry was also used to assess more fundamental parameters such as activation energy or diffusion mechanisms [31, 32]. Such studies were usually completed by density measurements and SEM observations that allowed the authors to evaluate the final microstructure of the pellets. In these conditions, several parameters of interest, such as grain size, pore size and distribution were determined *ex situ*, i.e. after the heat treatment aiming to the densification of the sample. Recently, several efforts were made to develop instrumentation methods able to monitor *in situ* the development of the microstructure, mainly through microscopic or tomographic observation performed directly during the heating step of the sample.

In this framework, High Temperature Transmission Electron Microscopy (HT-TEM) could provide precious details about the crystal organization within both grains and grain boundaries [33]. However, it remains too local to provide quantitative data that account for the whole sample. On the other hand, X-ray Tomography appears as a powerful tool which makes it possible to reconstruct the microstructure of the sample in 3D. Nevertheless, it appears to be limited by acquisition duration and spatial-resolution which were frequently found to be incompatible with the kinetics of diffusion phenomena leading to densification and grain growth [34, 35]. On this basis, we chose to develop since several years the *in situ* observation of the sintering of ceramic materials of interest for the nuclear fuel cycle using High Temperature Environmental Scanning Electron Microscopy (HT-ESEM). This review paper presents the different possibilities arising from this experimental technique at various scales. First, the results obtained from bulk pellets will be detailed, either regarding original fundamental data at the grain level (such as grain boundaries and pores motion), or design of dedicated microstructures through the assessment of grain growth kinetics. Acquisition of sintering maps thanks to the combination of HT-ESEM observations and classical dilatometric measurements will also be addressed. In a second part, observations undertaken at the 2-grains scale to monitor the first stage of sintering, dedicated to neck elaboration, will be presented, and compared to the results currently provided by the numerical models.

2. Experimental

2.1. Preparation of oxide powders with controlled morphologies

As it was stated previously, the powders used in current nuclear fuel fabrication processes are mainly issued from dry chemistry routes. In order to increase the control of several physico-chemical properties of the starting compounds, such as cation distribution, grain size, morphology, … novel wet chemistry methods have been employed. They are generally based on the precipitation of low-temperature precursors which are further converted into MO_2 fluorite-type dioxides through heat treatment at high temperature under appropriate atmosphere. Depending on the aim of the sintering studies undertaken *in situ*, various ways of preparation of the dioxides were then considered.

As a matter of example, SEM micrographs of UO_2 powders obtained from three different protocols are gathered in the **Figure 1**. The first sample depicted was obtained from oxalic precipitation [20], and can be considered as a reference owing to the large interest paid to this family of compounds by the community for almost one century [18]. In this case, a large excess of oxalic acid was added to a hydrochloric solution of U(IV), leading to the formation of $U(C_2O_4)_2.6H_2O$ [36]. This latter presents the classical square-shaped morphology of An(IV) oxalates which is further conserved during the transition towards UO_2 [37]. However, as this platelet habit appeared hardly suitable for densification, complementary mechanical treatments, such as ball milling, were frequently applied.

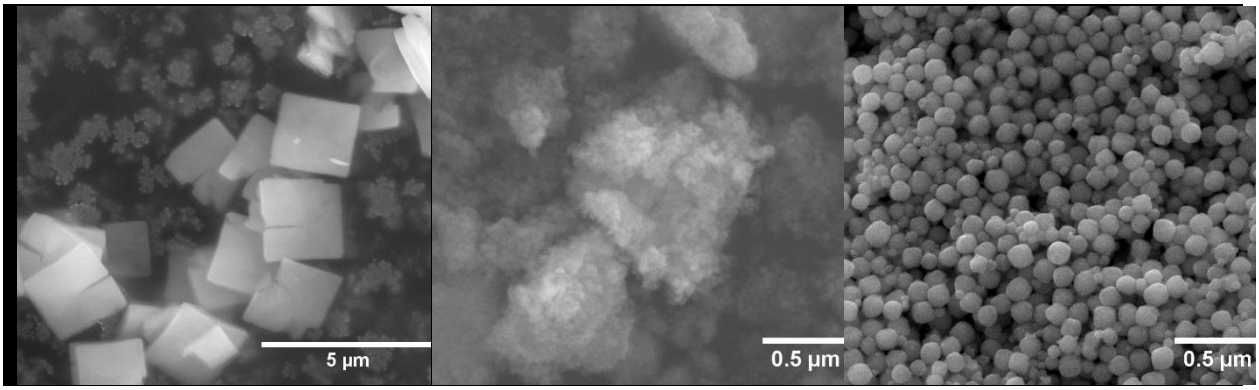

Figure 1. Scanning electron micrographs of UO_2 powders prepared from oxalic precipitation [20], hydroxide route [38], or precipitated from a mixture of U(IV) and urea [39].

More recently, other original precipitation routes of uranium(IV) dioxide were described in the literature. For example, highly reactive hydrated $UO_2.2H_2O$ powder was

obtained from the precipitation of tetravalent uranium in hydrochloric solution with ammonia, the resulting powder being later dried under stirring and vacuum [38]. Wet chemistry routes were also used for improving control over the final morphology of the powder. In this case, the transposition of synthesis methods initially designed for lanthanides-based compounds led to $UO_2.2H_2O$ microspheres [39]. These latter were obtained by using urea as a precipitating agent, with temperature and ageing time directly controlling the particles size.

Based on this wide range of preparation routes, it was then possible to achieve distinct morphologies, generally associated to very different reactivity. As a matter of example, the specific surface area of an oxide produced from hydroxide route can reach up to 100-150 $m^2.g^{-1}$, while it is usually less than 10 $m^2.g^{-1}$ from oxalic precipitation. Also, the final purity of the samples can be impacted, particularly through the presence of residual carbon after the thermic conversion of organic-based precursors such as oxalates [20]. It was then possible to adapt the preparation method to each kind of study envisaged. Hence, the preparation of MO_2 microspheres was considered to assess the first step of the densification process, which is usually modelled by two spherical grains in contact [26]. On the other hand, the sintering of bulk pellets was investigated with highly reactive powders, which can provide low sintering temperature easily accessible by HT-ESEM. Samples prepared from the initial precipitation of oxalate precursors were then favored, and eventually treated mechanically (typically through ball milling) before shaping.

2.2. *In situ* and *ex situ* ESEM observations

In situ observations of sintering phenomena were performed with a FEI Quanta 200 ESEM field-emission gun equipped with a 1500°C HT stage. Samples were directly placed in a MgO crucible coated with platinum. For the observation of bulk materials, a green pellet was first shaped by uniaxial pressing : depending on the powder used, applied pressure was adjusted between 100 and 500 MPa in order to reach a green density in the 40-50% range. Green pellets were then fractured into small pieces, one of them, with a size of about 100×100×100 μm^3, being selected then simply deposited in the HT stage crucible. On the other hand, the spherical particles used for monitoring the first stage of sintering were first dispersed in acetone then deposited onto a Pt-Au10 thin foil, further inserted in the HT-stage.

In both cases, the chamber was evacuated then filled with the adequate gas after insertion of the sample into the crucible. The observations were usually performed under 100-

200 Pa of selected atmospheres, including water vapour, air or helium. A specific detector was then used for *in situ* gaseous secondary electron imaging at high temperature (GSED). The samples were further rapidly heated (30-50°C.min^{-1}) up to the desired temperature then maintained isothermally in the ESEM chamber all along the experiment. Depending on the nature of the material and on the sintering stage analysed, temperatures ranging from 1000 to 1400°C were considered. The temperature of the sample was continuously measured using a homemade sample holder [40].

Micrographs were then regularly recorded during the heat treatment on a selected location of the sample at different magnifications. In order to overcome the problems associated to the loss of electronic contrast coming from the black body emission and to enhance the electronic emissions carrying information (i.e. SE and BSE), the accelerating voltage was increased to 30kV. Similarly, the current of the electron beam should be maximized. Finally, a working distance in the 19.5 to 21 mm range was selected due to the size of the furnace and of the heat shield.

Complementary *ex situ* experiments were also performed in conventional ovens in order to confirm that the electronic beam and/or the sampling did not affect the densification processes during *in situ* observations. In this case, samples were rapidly introduced in a furnace pre-heated at the required temperature and maintained at this temperature for a few minutes to several hours. SEM images were then recorded in both secondary and backscattered electron modes. When observing neck elaboration during microspheres sintering, such a process allowed one to follow both the morphological changes occurring on a single particle and to record images on a significant number of spherical particles (up to 30), leading to statistical data on a representative population.

2.3. Image processing

The main quantitative parameter extracted from the observation of bulk pellets during their densification concerns the evolution of the average grain size. In this aim, the image series were first treated by drawing manually the grain boundaries using the Gimp software [41], as the images contrast was generally not suitable for automated image processing. From 50 to 500 grains were systematically considered, depending on image quality and heat treatment duration [42]. On this basis, the data obtained after heating at the highest temperatures were usually associated to a high uncertainty due to the important grain growth

in the sample. The equivalent disc diameter was then defined as the relevant parameter for size evaluation and was determined using the ImageJ software [43].

When studying neck elaboration during microspheres sintering, the SEM images recorded *in situ* were processed following a two-step procedure (Figure 2). First, the extraction of the grain contours was processed using the Fiji software [43] and the specific Trainable Weka Segmentation plugin [44]. Then, these images were used for the direct determination of several parameters generally computed in the two-grain models describing the morphological modifications occurring during the first stage of sintering [45]. Custom software ImageJu was then developed [46] and allowed the direct determination of neck and grain radii, distance between the centers of the grains, neck radius of curvature and dihedral angles.

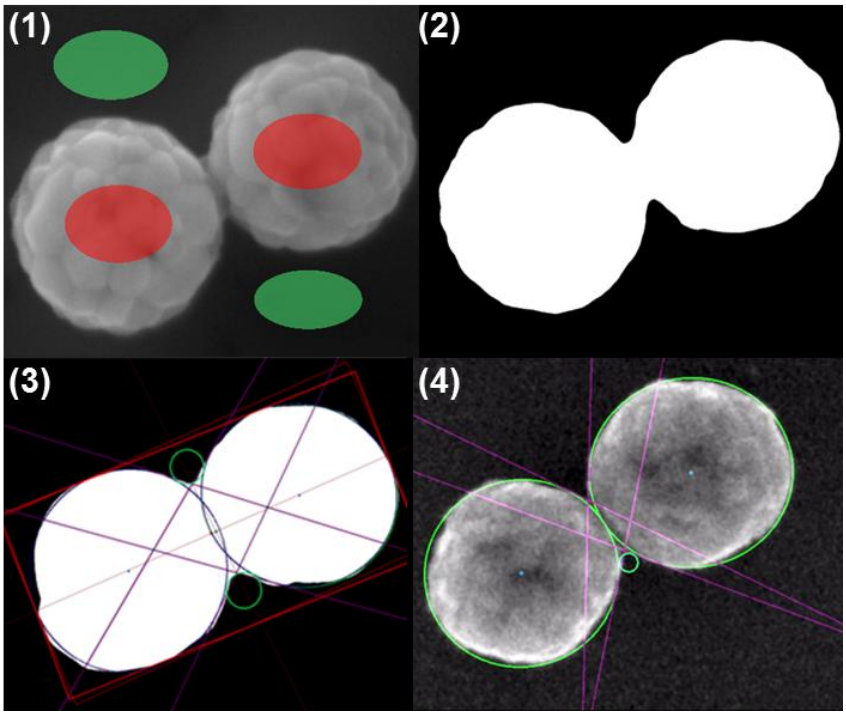

Figure 2. HT-ESEM images processing for the study of the initial stage of MO_2 microspheres sintering : binarization of the image (1), extraction of the contours (2), determination of parameters of interest (3) and final correspondence with initial micrograph (4).

3. Results and discussion

3.1. Determination of grain growth dynamics

The first investigations undertaken *in situ* through HT-ESEM were dedicated to the sintering of bulk materials and aimed to determine grain growth kinetics. In this purpose, the densification of MO_2 materials was studied during isothermal heat treatment at various temperatures. The Figure 3 presents the image series recorded during the sintering of ThO_2 at 1400°C, and constitutes a characteristic example of the data obtained.

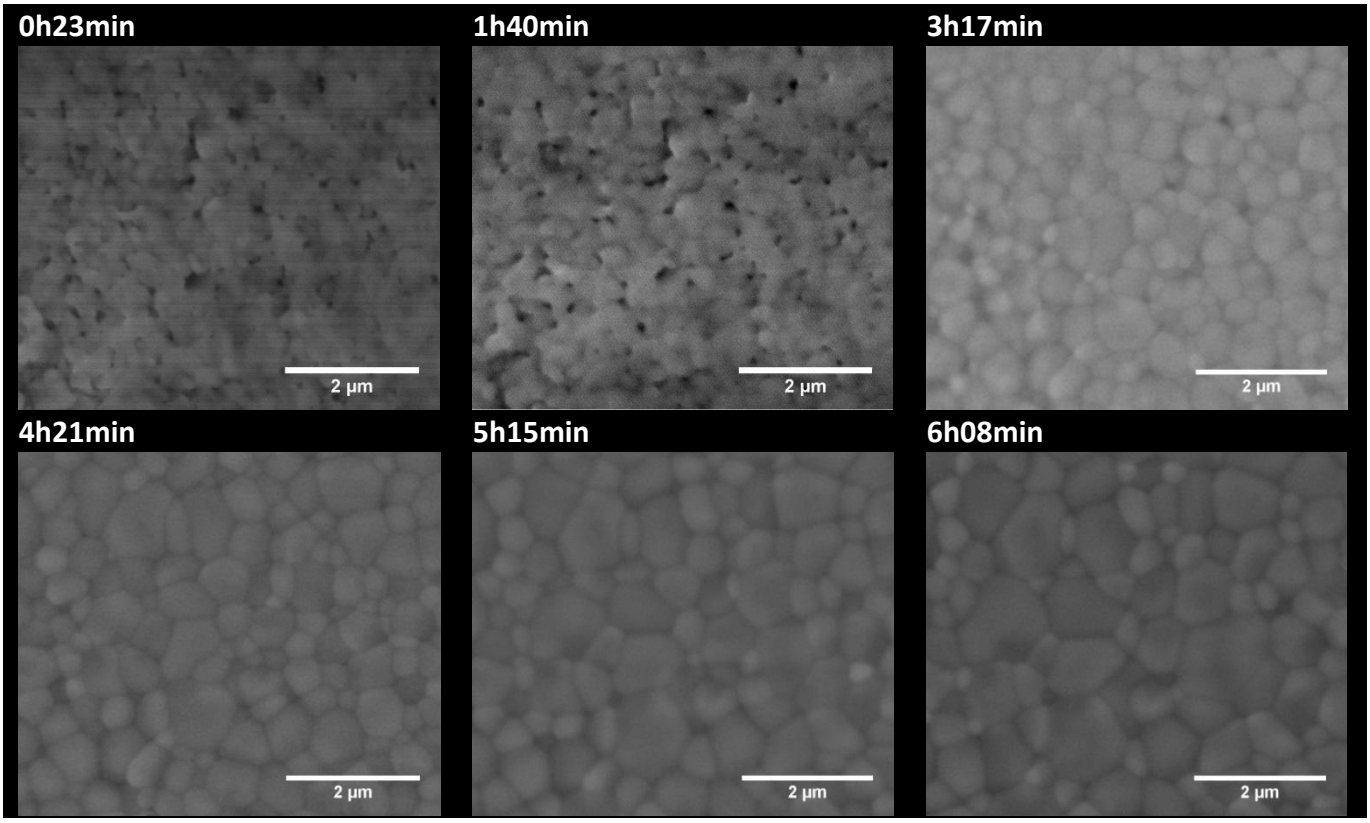

Figure 3. Selected HT-ESEM images collected *in situ* during the sintering of ThO_2 at T = 1400°C .

The comparison of the micrographs collected clearly enables one to directly observe the evolution of the microstructure of the sample. This latter is particularly evidenced by a significant increase in the average grain size, operated through the elimination of the smallest grains to the benefit of the biggest ones. Such mechanism, which was commonly described by densification models, and sometimes referenced as Ostwald ripening, was rarely observed *in situ* during the sintering of ceramic materials, especially actinide-bearing ones. Beyond the qualitative description of the topological evolution of the oxide systems during the sintering step, the acquisition of time-resolved micrographs of a dedicated zone of the sample allowed us to extract quantitative data linked with the development of the microstructure, such as grain growth rates or grain boundaries mobilities, in the intermediate and final stages of sintering (i.e. when grain growth and densification are strongly accelerated). Complementarily, *ex situ*

observations were systematically undertaken in order to get some preliminary insights into the initial stage of the sintering, and check that no effect related to the electron beam or to the sampling influenced the densification.

The most immediate information that can be issued from the micrographs deals with the evolution of the average grain size at the surface of the sample. An example is provided on **Figure 4**, which compares grain growth kinetics during the sintering of CeO_2 and ThO_2 ceramics at 1300°C [47, 48]. Such data can then be fitted using the general law of grain growth in pure and single phase ceramics which expresses the variation of the average grain radius according to :

$$G^n - G_0^n = k\,t \qquad (1.)$$

where G is the average grain size at time *t*, G_0 the average initial grain size and *n* an exponent characteristic of the process driving the grain growth [49].

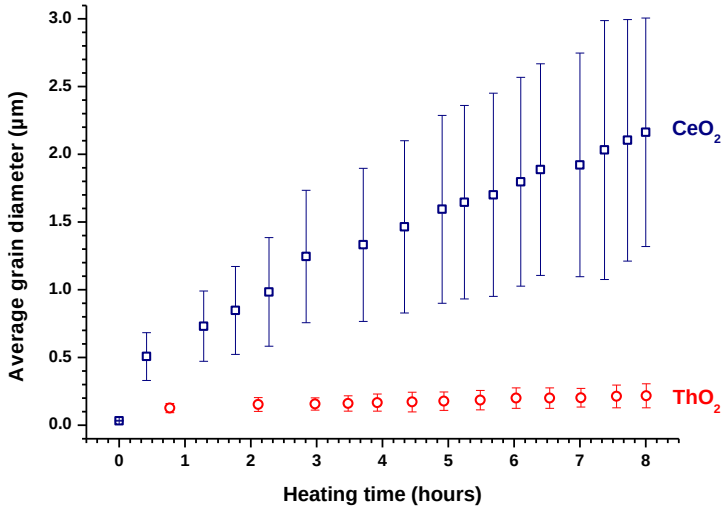

Figure 4. Evolution of the average grain size during the sintering of CeO_2 [47] and ThO_2 [48] samples at T = 1300°C under air atmosphere.

From these results, the range of temperature usually accessible thanks to HT-ESEM appeared to be perfectly suited for the study of the sintering of CeO_2. Indeed, whatever the operating conditions chosen between 1000°C and 1300°C, the *n* value was found to be close to 2, thus indicating a grain growth mechanism controlled by the grain boundaries mobility (regular grain growth). Conversely, the sintering of ThO_2 samples in a similar range of

temperature usually led to observe a linear trend in the variation of the average grain size (even though not through the origin), generally assigned to an exaggerated growth regime [50]. Nevertheless, such a process should also be evidenced by the separation of pores and grain boundaries, leading to the creation of intragranular porosity, which was never observed in this study. In these conditions, the more likely option is that the slow grain growth kinetics determined for ThO_2 sintering in the range of temperature studied only allowed us to observe the beginning of the phenomena. The differences in the kinetics measured were then correlated to the gap between optimal temperatures of sintering reported in the literature for both solids which range from 1100-1350°C for CeO_2 [51-53] to 1400-1500°C for ThO_2 [23, 54, 55]. HT-ESEM observations then have to be used in a convenient range of temperatures in order to thoroughly determine grain growth kinetics and associated mechanisms. On this basis, actinide dioxides, which usually presents a high sintering temperature (typically above 1500°C), can still be investigated, provided the use of highly reactive powders, obtained from mechanical treatments (ball milling, attrition, …) or from dedicated ways of synthesis, that generally lead to a significant decrease of the sintering temperature [22-24].

Once properly undertaken, the study of grain growth kinetics at various temperatures also led to the determination of activation energies. In this aim, the changes in ln (k) were plotted versus reciprocal temperature in Arrhenius diagrams, and led to new sets of values for fluorite-type MO_2 oxides. The examination of the data reported in the literature for these compounds (**Table 1**) reveals very scattered values. If some of these variations can be easily explained due to experimental conditions (for example from the influence of atmosphere for redox-sensitive samples), several discrepancies remain. They can be mainly linked with the method used for the determination of activation energy or to the way of preparation of the samples used. Also, the majority of the methods used is based on dilatometry measurements and frequently investigate different ranges of temperature. Different stages of the sintering process, going from initial formation of necks between the grains to grain growth and pore elimination, can then have been considered. The data reported thus possibly reflect different phenomena, sometimes overlapping one with each other.

In these conditions, the use of HT-ESEM observations for the determination of activation energies allowed to unambiguously assign the values obtained to pure grain growth. Also, in the case of ThO_2, where Th(IV) is the only stable oxidation state for this element, no contribution of redox reactions can be envisaged during the heat treatment (although recent results tend to evidence some differences in the mechanical properties of sintered ThO_2

depending on the atmosphere used [56]). The value of activation energy determined (435±25 kJ.mol^{-1} [48]) can thus be considered as a reference for other MO_2 compounds, including actinide dioxides such as AmO_2 for which the determination of experimental data is hardly accessible. Interestingly, it appeared to be in good agreement with some of the values reported for the sintering of CeO_2 in air (stabilization of tetravalent cerium) and for UO_2 under H_2 (stabilization of U(IV)), indicating that the activation energy of stoichiometric MO_2 fluorite-type compounds systematically lies around 400 kJ.mol^{-1}. Conversely, E_A can drop significantly when creating defects in the solids [31] : this is particularly the case when slightly oxidizing UO_2 into UO_{2+x} during the first stage of sintering, which can help to decrease the temperature required for complete densification [57].

Table 1. Values of activation energies reported in the literature for the sintering of various fluorite-type dioxides and determined through Master Sintering Curve (MSC), Constant Heating Rate (CHR), Rate Controlled Sintering (RCS) or Dorn's methods.

Sample	Atmosphere	Method	E_A (kJ.mol^{-1})	Reference
CeO_2	air	MSC	420 ± 10	[58]
	air		580	[59]
		CHR	365	[60]
	N_2	MSC	325	[61]
	air	*HT-ESEM*	*290 ± 40*	[47]
ThO_2			650	[62]
			625	[63]
	Ar-8%H_2	MSC	520	[54]
	air	*HT-ESEM*	*435 ± 25*	[48]
$UO_{2.00}$	H_2	CHR	429 ± 8	[31]
	H_2	Dorn	420	[64]
	N_2-5%H_2	RCS	287	[32]
$UO_{2.09}$	H_2	CHR	242 ± 6	[31]
$UO_{2.17}$	H_2	CHR	299 ± 9	[31]
$(U_{0.5}Pu_{0.5})O_2$	Ar-8%H_2	CHR	376	[30]
	CO_2	CHR	138	[30]
PuO_2	Ar	CHR	210	[65]
	Ar-8%H_2	CHR	159	[65]

3.2. Kinetics associated to local phenomena

Along with global data determined from the observation of hundreds of grains at the surface of ceramic sample during the sintering process, the high resolution of HT-ESEM images, even when operating at high temperature, can be used to assess local kinetic data associated to the motion of grain boundaries and to the elimination of pores.

As there is no static reference at the surface of the sample, the velocity of the grain boundaries was determined from the evolution of the distance separating two opposite grain boundaries (*i.e.* face to face one with each other). Whatever the oxide compound studied, the values obtained were generally determined for 5-10 couples of grain boundaries and systematically found in the 0-5 $\mu m.h^{-1}$ range, which constitutes a first evaluation for ceramic materials. Indeed, the mobility of grain boundaries was up to now mainly assessed in metals, where values of several hundreds of $\mu m.h^{-1}$ are usually reported [66, 67]. The Figure 5, which presents the evolution of grain boundaries velocities during the sintering of CeO_2 or ThO_2 at 1400°C, clearly reveals that different cases can be observed depending on the grain considered. As it was expected from the description of grain growth in the literature, some grains grow during heat treatment while the smallest ones tend to disappear. Nevertheless, very sudden variations can occur in the evolution of a given grain, mainly due to its dynamic environment. The number of neighbors, the grain boundaries curvature, as well as the concentration of defects eventually present within the grains can be responsible for these variations [68, 69]. Also, it is interesting to see that this evolution is not systematically linear : whatever the oxide studied, some grains were found to initially expand then finally shrink, or inversely. This observation contradicts the predictions made by several theoretical models such as that of Wakai [70] who reported a similar rate of elimination for all the grains in the solid.

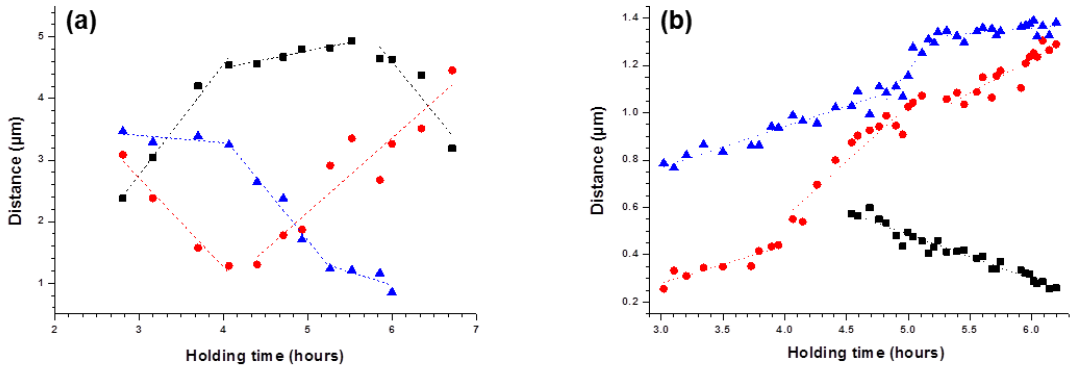

Figure 5. Evolution of distances separating two opposite grain boundaries during the sintering of CeO_2 [71] (a) and ThO_2 [48] (b) at T = 1400°C. The various colors illustrate different grains randomly considered for each system.

The elimination of porosity was also observed on the micrographs series recorded at high temperature. Such a phenomenon was commonly foreseen for intergranular pores located at the grain boundaries. Indeed, these latter are generally dragged by the motion of the

boundaries to finally merge together and be eliminated concomitantly to grain growth. More surprisingly, the observation of CeO_2 samples during sintering also presented the elimination of some closed pores, initially located within the grains themselves [71]. Intragranular pores are usually formed through pore detachment from the grain boundaries [72, 73]: they are then represented as spherical pores embedded in the grains, with no remaining driving force promoting their motion. Intragranular pores are then hardly removable from the solid and frequently associated with the end of the densification process. The use of HT-ESEM for the *in situ* observation of the sintering of ceramic materials here appeared as a unique opportunity to image the elimination of closed porosity, which remained a surface-only phenomenon. Indeed, the pore displacement should be linked to gradients from the bulk to the surface of the pellet, either regarding temperature or Ce/O stoichiometry or anisotropic pressure in the solid matrix in the vicinity of pore [74]. A mathematical treatment was then applied to the image series to reconstruct the pore trajectory inside the solid. The extraction of the grey-level curves using ImageJ software was performed on each image along a line which goes through the pore diameter. The obtained curves were then interpreted regarding to the pore position relatively to the sample surface. By these means, it was then possible to measure the pores velocities as a function of their size : above 500 nm, pore displacement was typically limited to 0.5 $\mu m.h^{-1}$ while it reached more than 1 $\mu m.h^{-1}$ for pore diameters below 400 nm [71]. In this case, HT-ESEM observations led to results in good agreement with theoretical models, which described pore displacement as a function of k/r^n, where k is the kinetic constant, r the pore diameter, and n the exponent characteristic of the diffusion mechanism involved [75].

3.3. Rapid acquisition of sintering maps

The sintering map of a ceramic reports the variation of the average grain size as a function of the relative density of the samples. It is generally used to tailor the final microstructure of the material for various operating conditions, that can include temperature, heating time, atmosphere, … [42, 76] Due to the time needed for their acquisition, which requires an important number of heat treatments followed by density measurements and SEM observations/images analysis, sintering maps were very rarely, if never, reported for actinide-bearing materials, although some authors tried to forecast the microstructural evolution of UO_2 during sintering from numerical models [77, 78]. On this basis, an original approach based on the joint utilization of HT-ESEM observations and dilatometric measurements was

designed to give a fast access to ThO_2 sintering map [48]. In this aim, the relative density of the pellet was calculated from the relative linear shrinkage measured by dilatometry during isothermal heat treatment, assuming that the sintering was strictly isotropic. On the other hand, the average grain size was directly extracted from the image analysis of HT-ESEM micrographs recorded *in situ*, as presented previously. The combination of both data sets led to sintering trajectories for all the temperatures investigated, which can be gathered together as a sintering map (Figure 6).

Such a curve clearly revealed that the microstructural development of the ThO_2 ceramic occurred in two steps. The first one is mainly dedicated to the densification of the sample : while the relative density increased from 70 to almost 92%, the average grain size only appeared slightly modified. This densification process could be linked to the initial and intermediate stages of sintering, *i.e.* to the formation of necks between the grains then to the elimination of the open porosity [25, 26]. Thereafter, an almost constant value of the relative density was reached (around 93-94%), and the average grain size increased strongly. This grain growth step can then be linked to the final stage of sintering, where the presence of remaining closed pores can inhibit the densification process, but still allowing grain growth to pursue.

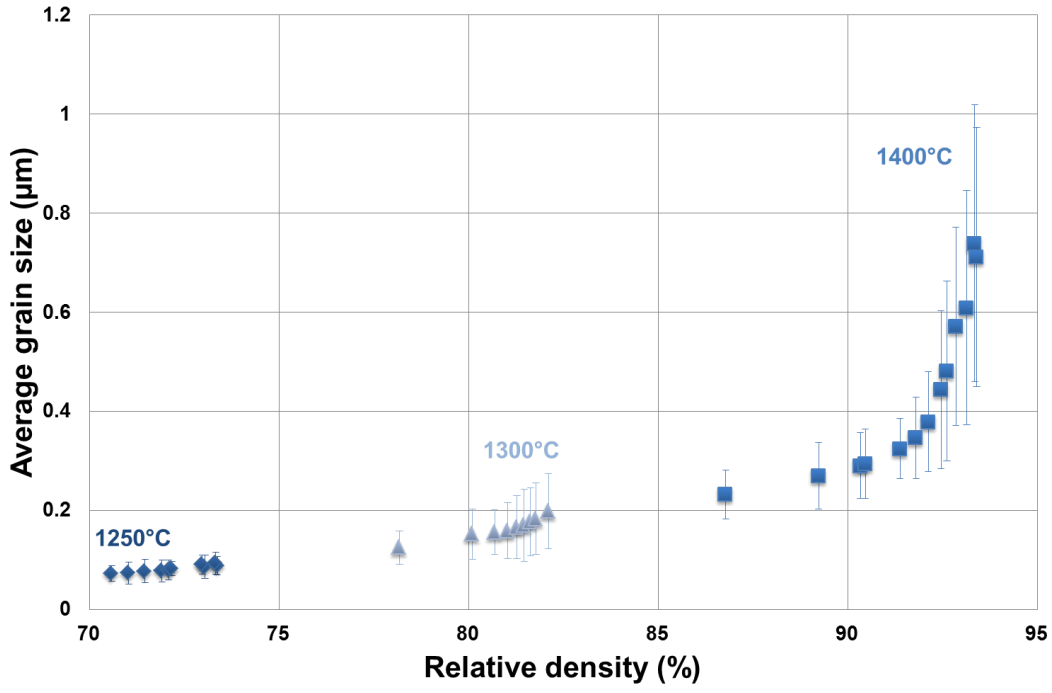

Figure 6. Sintering map of ThO_2 determined from the combination of HT-ESEM and dilatometry data [48].

The sintering map also demonstrated that dense AnO_2 ceramics presenting original microstructures can be obtained through the use of wet chemistry routes involving the precipitation of low-temperature precursors. Indeed, in the case of ThO_2, the initial preparation of thorium oxalate to produce ThO_2 nanopowders after pre-heating and grinding steps allowed producing dense pellets constituted by small grains : after 6 hours at 1400°C, the average grain size remained submicrometric, which was generally correlated to an improved mechanical behaviour. Also, the sintering map can be used efficiently to tune the porosity amount in the ceramic samples, which often appeared as a key-parameter in the nuclear fuel requirements. The use of HT-ESEM to rapidly acquire sintering maps could then be considered as a promising opportunity to yield original fuel ceramics, notably in the framework of the development of new generations of nuclear reactors [79].

3.4. Investigation of the first step of sintering

The observation of bulk pellets during their heat treatment at high temperature through HT-ESEM allowed us to image the various phenomena linked with the intermediate and final stages of sintering, *i.e.* grain growth and pore elimination. However, the small average grain size of the powders used (typically below the micrometer scale), associated to the important displacement of the sample during heating ramp, preclude the observation of the first step of sintering, which is marked by the formation of necks between the grains. In order to get original insights on this key-step of the densification process, which confers a mechanical strength to the powder agglomerate, dedicated powders were prepared (see above). Indeed, the models describing the first step of sintering are usually based on two spheres in contact supposed to be single-crystals. The behavior of comparable microspheres was then assessed versus temperature for CeO_2 and ThO_2 samples.

As the grains synthesized were initially polycrystalline, the first step of this work dealt with the evolution of the microspheres inner structure when heating [80]. The variation of the average size of the crystallites composing the microspheres (which must not be confused with grain growth within a compact) was then measured by various means, including HT-ESEM *in situ* observations, ESEM *ex situ*, and complementary Rietveld refinement of the PXRD patterns of thermally treated powders (Figure 7). As illustrated by the HT-ESEM micrographs presented, the microspheres progressively shifted from a polycrystalline arrangement to an almost spherical single crystal. Also, the crystallite growth kinetics was found to follow a two-exponential model. The determination of associated activation energies led to conclude to

two distinct mechanisms driving the microsphere evolution. For short heating time, a low value of E_A (typically below 100 kJ.mol^{-1}) was associated to the mechanical rearrangement of crystallites, also known as "oriented attachment" [81]. Conversely, for long heating times, the value of activation energy reached several hundreds of kJ.mol^{-1} and was associated to solid state diffusion. Such values also appeared in good agreement with those usually reported for sintering of bulk materials and gathered herein in Table 1. Moreover, the relative importance of these two mechanisms was found to vary depending on the way of preparation of the microspheres. Indeed, when the samples were initially precipitated as low-temperature precursors, then fired to yield the desired oxide, a residual mesoporosity [82] was detected in the microspheres, and was found to promote oriented attachment. On the other hand, the direct precipitation of oxides, which was correlated to much denser microspheres was usually more in favor of solid state diffusion [83]. The study of individual grains versus temperature then appeared to provide important information concerning the different mechanisms operating during the heat treatment. Also, it allowed us to determine precisely the conditions of preparation (both in terms of heating time and temperature) of spherical single crystals that could further be used to mimic the systems generally modelled and compare their behavior to polycrystalline samples.

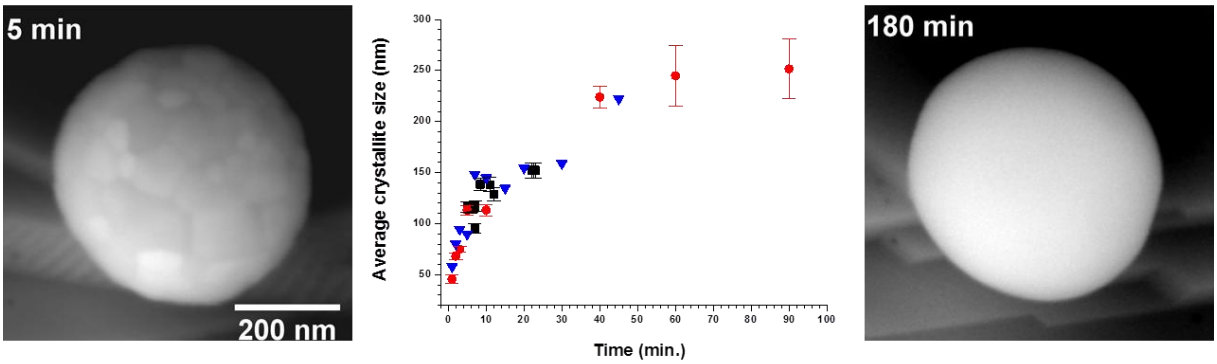

Figure 7. Evolution of the average crystallite size in CeO_2 microspheres during heat treatment at 1100°C, determined from *in situ* (■) and *ex situ* (●) ESEM data, and PXRD Rietveld refinement (▼). HT-ESEM micrographs represent initial polycrystalline sample and spherical single crystal obtained at the end of the heat treatment (scale bar stands for both) [80].

The behavior of two microspheres in contact was then investigated in various operating conditions for polycrystalline or single crystal samples. For both systems, a neck between the microspheres was first formed and then grew continuously. Same modifications occurred whatever the sintering temperatures studied in the 1100°C-1225°C range, but with different kinetics. Also, these latter were systematically enhanced when working with

polycrystalline grains. In this case, neck growth was simultaneously accompanied by the gradual decrease of the crystallites number within the grains, as evidenced by the micrographs series reported on Figure 8.

For both polycrystalline and single-crystal microspheres, the evolution of the grain assembly was described through :

$$\lambda = x/r \qquad (2.)$$

Where λ is a dimensionless parameter usually referred to as the sintering advancement, x the radius of the neck formed between the two microspheres and r the radius of the microspheres considered.

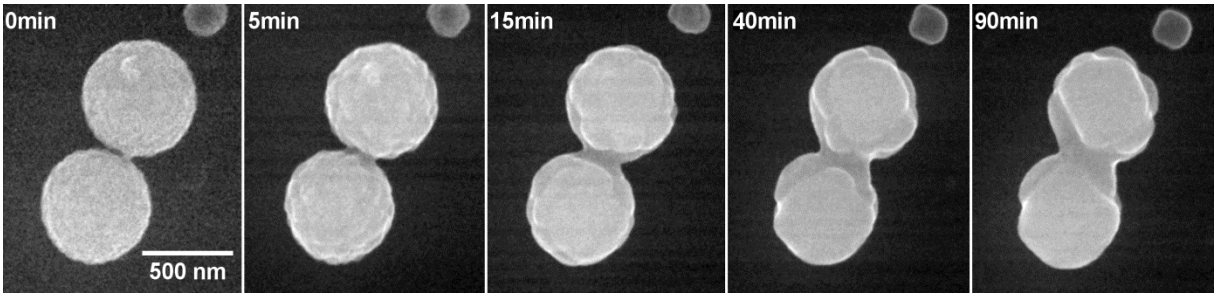

Figure 8. *In situ* HT-ESEM observation of CeO_2 polycristalline microspheres sintering at 1100°C.

Moreover, for single-crystals, the evolution of the λ parameter during neck growth was described since the 1960s by several authors, and can be modelled by the simple law :

$$\lambda = \left(\frac{k.t}{r^m}\right)^{1/n} = (k'.t)^{1/n} \qquad (3.)$$

where k is the kinetic constant, and n and m are exponents characteristic of the diffusion mechanism involved in neck growth [45, 84]. As the HT-ESEM observations performed on our systems revealed that the grain sizes remained almost unchanged, it was then possible to directly determine a new kinetic constant k', and to deduce the value of n from the data collected (Figure 9).

The activation energies evaluated from the variation of ln (k) versus the reciprocal temperature always led to values in the 400-600 $kJ.mol^{-1}$ range. Once again, these values appeared in good agreement with those reported for the sintering of bulk materials. Moreover, when compared with data coming from the study of isolated microspheres, they tend to show that only solid state diffusion is operating during the elaboration of neck in single crystal

systems. Consequently, the n value was determined from the variation of λ and was systematically found close to 6, indicating a neck growth controlled by grain boundary diffusion [85]. For polycrystalline systems, the obtained data were modelled by a simple exponential function, as no model was available in the literature. The activation energies determined were then found to be significantly lower than for single crystals (typically around 200 kJ.mol^{-1}) and revealed that the mechanical rearrangement of the crystallites in the neck region operates concomitantly with solid state diffusion. Also, the important number of boundaries between crystallites probably acts as short-circuits for solid-state diffusion.

In order to evaluate the impact of such a difference of mechanism on the validity of models, the experimental results obtained for CeO_2 were compared with data computed through the SALAMMBO code [27, 28]. For the single crystal particles, a very good correlation was found between the two sets of data (Figure 9). Indeed, the evolution of the sintering degree followed a similar trend despite slight differences in the absolute values of *y*, which could mainly be assigned to the non-ideal morphology of the particles used in the experiments. Conversely, the simulated curve exhibited a significant deviation from the polycrystalline particles, which can obviously be considered as closer to real materials. This difference then clearly underlines the influence of the polycrystallinity of the grains on the sintering evolution : correlatively, it also indicates that current mathematical models only provide qualitative guidelines, but will not result in a reliable and quantitative prediction of the sintering degree evolution and morphology's variation.

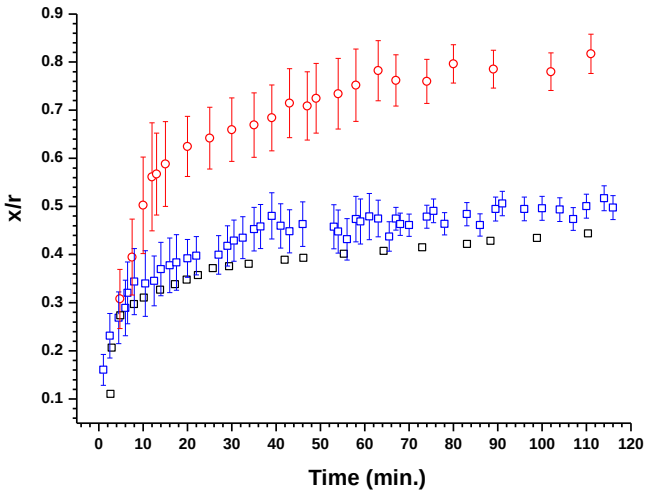

Figure 9. Comparison between experimental results and modeling during sintering of two CeO_2 microspheres at 1100°C : polycrystalline samples (○), single crystals (□) and results from the SALAMMBO model (□) [85].

4. Conclusion

The various results obtained from HT-ESEM experiments showed that a wide range of data can be deduced from the *in situ* observation of ceramic samples during their densification. They both deal with fundamental information, such as the nature of the mechanisms involved, diffusion path, or associated activation energies, and practical guidelines that can be directly used to tailor the final microstructure of a material. In this sense, HT-ESEM appears as a versatile tool, where the sintering temperature and atmosphere can be easily tuned. Moreover, the amount of sample needed to investigate the densification phenomena is limited, making the techniques perfectly suitable for the study of radioactive materials. Finally, the data obtained by these means can be complemented by those collected from more conventional techniques, such as dilatometry, to easily yield to sintering maps, which could be used in the future to achieve original fuel microstructures in the framework of the Gen-IV reactors development [79].

Even if some drawbacks remain (operating temperature limited to 1400°C, surface-only information, …), the use of HT-ESEM can then be envisaged in the near future to get new insights into the densification of ceramics of interest for the nuclear fuel cycle. Particularly, the study of UO_2 has to be undertaken, with a special attention paid to the influence of the oxygen partial pressure in the direct environment of the sample. Special efforts also have to be made for mixed oxides, which can be used to mimic the behavior of MOx fuel during their manufacturing. In this case, beyond the parameters already studied for simple oxides, the impact of the sample homogeneity must be evaluated. Also, for such materials, the densification process will be accompanied by the formation of a solid solution, which can be used to determine interdiffusion coefficients.

Finally, beyond the study of densification processes, the evaluation of the life-cycle of nuclear ceramics requires to master and forecast the microstructural evolutions linked with other key-steps of the nuclear fuel cycle. This is particularly the case for alteration phenomena, either when dealing with the total dissolution of a fuel material during its reprocessing, or with the leaching of a ceramic wasteform in an underground repository. In both scenarios, it will be essential to point out eventual zones of weakness, which present a degraded chemical durability (triple jonctions, grain boundaries, ….), and to correlate their evolution to the monitoring of inventory of elements in solution [86]. The *in situ* observation of nuclear ceramics (especially incorporating actinides) in presence of a thin liquid alteration

layer at their surface, then indubitably constitutes the next challenge to complete, both from technical and scientific point of views, for environmental scanning electron microscopy.

Acknowledgements

Authors would like to thank J. Ravaux and H.P. Brau from ICSM for their help in the recording and the processing of HT-ESEM images, and J. Favrichon (CEA/DEN/UG-UST/STIC/GPSI) for the development of the ImageJu software. They are also grateful to the Materials Federative Project included in the NEEDS program (Nucléaire, Energie, Environnement, Déchets, Société) of CNRS and to CEA for their continuous financial support.

References

[1] Gelman, S.: Nuclear fuel research and fabrication. Atw-Internationale Zeitschrift Fur Kernenergie, **42**, 408-408 (1997).

[2] Hagi, S., Yamamoto, A., Matsuura, K.: Introduction to nuclear fuel engineering; Focused on LWR fuel - (8) LWR fuel fabrication, nuclear and thermal-hydraulic design. Journal of the Atomic Energy Society of Japan, **47**, 35-44 (2005).

[3] Ion, S.E., Watson, R.H., Loch, E.P.: Fabrication of Nuclear-Fuel. Nuclear Energy-Journal of the British Nuclear Energy Society, **28**, 21-28 (1989).

[4] Mori, K.: Introduction to nuclear fuel engineering, focused on LWR fuel - (7) LWR fuel fabrication. Journal of the Atomic Energy Society of Japan, **46**, 838-844 (2004).

[5] Berzati, S., Vaudez, S., Belin, R.C., Lechelle, J., Marc, Y., Richaud, J.C., Heintz, J.M.: Controlling the oxygen potential to improve the densification and the solid solution formation of uranium-plutonium mixed oxides. Journal of Nuclear Materials, **447**, 115-124 (2014).

[6] Fisher, S.B., White, R.J., Cook, P.M.A., Bremier, S., Corcoran, R.C., Stratton, R., Walker, C.T., Ivison, P.K., Palmer, I.D.: Microstructure of irradiated SBR MOX fuel and its relationship to fission gas release. Journal of Nuclear Materials, **306**, 153-172 (2002).

[7] Abe, T., Asakura, K., Uranium oxide and MOX production, in: R.J.M. Konings, T.R. Allen, R.E. Stoller, S. Yamanaka (Eds.) Comprehensive nuclear materials, Elsevier, Amsterdam, 2012, pp. 393-422.

[8] Kutty, T.R.G., Hegde, P.V., Khan, K.B., Basak, U., Pillai, S.N., Sengupta, A.K., Jain, G.C., Majumdar, S., Kamath, H.S., Purushotham, D.S.C.: Densification behaviour of UO_2 in six different atmospheres. Journal of Nuclear Materials, **305**, 159-168 (2002).

[9] Song, K.W., Kim, K.S., Kim, Y.M., Jung, Y.H.: Sintering of mixed UO_2 and U_3O_8 powder compacts. Journal of Nuclear Materials, **277**, 123-129 (2000).

[10] Bourgeois, L., Dehaudt, P., Lemaignan, C., Hammou, A.: Factors governing microstructure development of Cr_2O_3-doped UO_2 during sintering. Journal of Nuclear Materials, **297**, 313-326 (2001).

[11] Kim, K.S., Yang, J.H., Jung, Y.H., Song, K.W., Kang, K.W., Kim, K.M.: Sintering Behavior of Cr_2O_3-doped UO_2 Pellets. Nuclear Engineering and Technology, **35**, 14-24 (2003).

[12] Harada, Y.: Sintering behaviour of niobia-doped large grain UO_2 pellet. Journal of Nuclear Materials, **238**, 237-243 (1996).

[13] Song, K.W., Kim, S.H., Na, S.H., Lee, Y.W., Yang, M.S.: Effects of Nb_2O_5 addition on grain-growth and densification in UO_2 pellets under reducing and/or oxidizing atmospheres. Journal of Nuclear Materials, **209**, 280-285 (1994).

[14] Oudinet, G., Munoz-Viallard, I., Aufore, L., Gotta, M.J., Becker, J.M., Chlarelli, G., Castelli, R.: Characterization of plutonium distribution in MIMAS MOX by image analysis. Journal of Nuclear Materials, **375**, 86-94 (2008).

[15] Kutty, T.R.G., Hegde, P.V., Khan, K.B., Majumdar, S., Purushotham, D.S.C.: Sintering studies on UO_2-PuO_2 pellets with varying PuO_2 content using dilatometry. Journal of Nuclear Materials, **282**, 54-65 (2000).

[16] Krellmann, J.: Plutonium Processing at the Siemens Hanau Fuel Fabrication Plant. Nuclear Technology, **102**, 18-28 (1993).

[17] Grandjean, S., Arab-Chapelet, B., Robisson, A.C., Abraham, F., Martin, P., Dancausse, J.P., Herlet, N., Leorier, C.: Structure of mixed U(IV)-An(III) precursors synthesized by co-conversion methods (where An = Pu, Am or Cm). Journal of Nuclear Materials, **385**, 204-207 (2009).

[18] Abraham, F., Arab-Chapelet, B., Rivenet, M., Tamain, C., Grandjean, S.: Actinide oxalates, solid state structures and applications. Coord. Chem. Rev., **266-267**, 28-68 (2014).

[19] Lebreton, F., Horlait, D., Delahaye, T., Blanchart, P.: Fabrication and characterization of $U_{1-x}Am_xO_{2+\delta}$ compounds with high americium contents (x=0.3, 0.4 and 0.5). Journal of Nuclear Materials, **439**, 99-102 (2013).

[20] Martinez, J., Clavier, N., Ducasse, T., Mesbah, A., Audubert, F., Corso, B., Vigier, N., Dacheux, N.: From uranium(IV) oxalate to sintered UO_2: Consequences of the powders' thermal history on the microstructure. Journal of the European Ceramic Society, **35**, 4535-4546 (2015).

[21] Ramond, L., Horlait, D., Delahaye, T., Jouan, G., Gauthe, A., Arab-Chapelet, B., Picart, S.: Dilatometric study of a co-converted $(U,Am)O_2$ powder. Journal of the European Ceramic Society, **36**, 1775-1782 (2016).

[22] Gao, J.H., Yang, X.D., Li, R., Wang, Y., Zhong, F.W.: Low-temperature sintering mechanism on uranium dioxide. Journal of Materials Science, **42**, 5936-5940 (2007).

[23] Hingant, N., Clavier, N., Dacheux, N., Hubert, S., Barre, N., Podor, R., Aranda, L.: Preparation of morphology controlled $Th_{1-x}U_xO_2$ sintered pellets from low-temperature precursors. Powder Technology, **208**, 454-460 (2011).

[24] White, G.D., Bray, L.A., Hart, P.E.: Optimization of Thorium Oxalate Precipitation Conditions Relative to Derived Oxide Sinterability. Journal of Nuclear Materials, **96**, 305-313 (1981).

[25] Kang, S.J.L., Sintering - Densification, Grain Growth & Microstructure, Burlington, 2005.

[26] Bernache-Assollant, D., Chimie-Physique du Frittage, Paris, 1993.

[27] Lechelle, J., Boyer, R., Trotabas, M.: A mechanistic approach of the sintering of nuclear fuel ceramics. Materials Chemistry and Physics, **67**, 120-132 (2001).

[28] Martin, S., Parekh, R., Guessasma, M., Lechelle, J., Fortin, J., Saleh, K.: Study of the sintering kinetics of bimodal powders. A parametric DEM study. Powder Technology, **270**, 637-645 (2015).

[29] Noyau, S., Audubert, F., Martin, P.M., Maitre, A.: Influence of the oxygen potential on the sintering of UO_2-45% PuO_2. Journal of the European Ceramic Society, **35**, 3651-3663 (2015).

[30] Kutty, T.R.G., Hegde, P.V., Keswani, R., Khan, K.B., Majumdar, S., Purushotham, D.S.C.: Densification behaviour of UO_2-50%PuO_2 pellets by dilatometry. Journal of Nuclear Materials, **264**, 10-19 (1999).

[31] Dehaudt, P., Bourgeois, L., Chevrel, H.: Activation energy of UO_2 and UO_{2+x} sintering. Journal of Nuclear Materials, **299**, 250-259 (2001).

[32] Lahiri, D., Rao, S.V.R., Rao, G.V.S.H., Srivastava, R.K.: Study on sintering kinetics and activation energy of UO_2 pellets using three different methods. Journal of Nuclear Materials, **357**, 88-96 (2006).

[33] Asoro, M.A., Kovar, D., Shao-Horn, Y., Allard, L.F., Ferreira, P.J.: Coalescence and sintering of Pt nanoparticles: in situ observation by aberration-corrected HAADF STEM. Nanotechnology, **21**, (2010).

[34] Kieback, B., Nothe, M., Banhart, J., Grupp, R.: Investigation of Sintering Processes by Tomography. Thermec 2009, Pts 1-4, **638-642**, 2511-2516 (2010).

[35] Nothe, M., Schulze, M., Grupp, R., Kieback, B., Haibel, A., Banhart, J.: Analysis of particle rearrangement during sintering by micro focus computed tomography (mu CT). Progress in Powder Metallurgy, Pts 1 and 2, **534-536**, 493-496 (2007).

[36] Duvieubourg-Garea, L., Vigier, N., Abraham, F., Grandjean, S.: Adaptable coordination of U(IV) in the 2D-(4,4) uranium oxalate network: From 8 to 10 coordinations in the uranium (IV) oxalate hydrates. Journal of Solid State Chemistry, **181**, 1899-1908 (2008).

[37] Hingant, N., Clavier, N., Dacheux, N., Barre, N., Hubert, S., Obbade, S., Taborda, F., Abraham, F.: Preparation, sintering and leaching of optimized uranium thorium dioxides. Journal of Nuclear Materials, **385**, 400-406 (2009).

[38] Martinez, J., Clavier, N., Mesbah, A., Audubert, F., Le Goff, X.F., Vigier, N., Dacheux, N.: An Original Precipitation Route toward the Preparation and the Sintering of Highly Reactive Uranium Cerium Dioxide Powders. Journal of Nuclear Materials, **462**, 173-181 (2015).

[39] Nkou Bouala, G.I., Clavier, N., Podor, R., Cambedouzou, J., Mesbah, A., Brau, H.P., Léchelle, J., Dacheux, N.: Preparation and characterisation of uranium oxides with spherical shapes and hierarchical structures. Crystengcomm, **16**, 6944-6954 (2014).

[40] Podor, R., Pailhon, D., Ravaux, J., Brau, H.P.: Development of an Integrated Thermocouple for the Accurate Sample Temperature Measurement During High Temperature Environmental Scanning Electron Microscopy (HT-ESEM) Experiments. Microscopy and Microanalysis, **21**, 307-312 (2015).

[41] GIMP - GNU Image Manipulation Program, www.gimp.org, accessed: 09.29.2016.

[42] Maitre, A., Beyssen, D., Podor, R.: Modelling of the grain growth and the densification of SnO_2-based ceramics. Ceramics International, **34**, 27-35 (2008).

[43] Rasband, W.: ImageJ software, Image processing and analysis in Java.

[44] Pascau, J., Mateos Perez, J.M., Image processing with ImageJ, Birmingham, UK, 2013.

[45] Coble, R.L.: Review of Diffusion Sintering Models and Their Applicability to Development and Processing. American Ceramic Society Bulletin, **50**, 754-& (1971).

[46] Imageju, https://github.com/jfavrichon/imageju, accessed: 09.29.2016.

[47] Podor, R., Clavier, N., Ravaux, J., Claparede, L., Dacheux, N.: *In Situ* HT-ESEM Observation of CeO_2 Grain Growth During Sintering. Journal of the American Ceramic Society, **95**, 3683-3690 (2012).

[48] Clavier, N., Podor, R., Deliere, L., Ravaux, J., Dacheux, N.: Combining *in situ* HT-ESEM observations and dilatometry: An original and fast way to the sintering map of ThO_2. Materials Chemistry and Physics, **137**, 742-749 (2013).

[49] Hillert, M.: On Theory of Normal and Abnormal Grain Growth. Acta Metallurgica, **13**, 227-& (1965).

[50] Carpay, F.M.A.: Discontinuous Grain-Growth and Pore Drag. Journal of the American Ceramic Society, **60**, 82-83 (1977).

[51] Baumard, J.F., Gault, C., Argoitia, A.: Sintered Ceria - a New Dense and Fine-Grained Ceramic Material. Journal of the Less-Common Metals, **127**, 125-130 (1987).

[52] Kleinlogel, C., Gauckler, L.J.: Sintering of nanocrystalline CeO_2 ceramics. Advanced Materials, **13**, 1081-1085 (2001).

[53] Zhou, Y.C., Rahaman, M.N.: Hydrothermal Synthesis and Sintering of Ultrafine CeO_2 Powders. Journal of Materials Research, **8**, 1680-1686 (1993).

[54] Kutty, T.R.G., Khan, K.B., Hegde, P.V., Banerjee, J., Sengupta, A.K., Majumdar, S., Kamath, H.S.: Development of a master sintering curve for ThO_2. Journal of Nuclear Materials, **327**, 211-219 (2004).

[55] Ananthasivan, K., Anthonysamy, S., Singh, A., Rao, P.R.V.: De-agglomeration of thorium oxalate - a method for the synthesis of sinteractive thoria. Journal of Nuclear Materials, **306**, 1-9 (2002).

[56] Baena, A., Cardinaels, T., Van Eyken, J., Puzzolante, J.L., Binnemans, K., Verwerft, M.: Effect of sintering atmosphere on the hardness of ThO_2. Journal of Nuclear Materials, **477**, 222-227 (2016).

[57] Harada, Y.: UO_2 sintering in controlled oxygen atmospheres of three-stage process. Journal of Nuclear Materials, **245**, 217-223 (1997).

[58] Kinemuchi, Y., Watari, K.: Dilatometer analysis of sintering behavior of nano-CeO_2 particles. Journal of the European Ceramic Society, **28**, 2019-2024 (2008).

[59] Chen, P.L., Chen, I.W.: Grain growth in CeO_2: Dopant effects, defect mechanism, and solute drag. Journal of the American Ceramic Society, **79**, 1793-1800 (1996).

[60] Zhang, T.S., Hing, P., Huang, H.T., Kilner, J.: Early-stage sintering mechanisms of Fe-doped CeO_2. Journal of Materials Science, **37**, 997-1003 (2002).

[61] de Florio, D.Z., Esposito, V., Traversa, E., Muccillo, R., Fonseca, F.C.: Master sintering curve for Gd-doped CeO_2 solid electrolytes. Journal of Thermal Analysis and Calorimetry, **97**, 143-147 (2009).

[62] Matzke, H.: On Uranium Self-Diffusion in UO_2 and UO_{2+x}. Journal of Nuclear Materials, **30**, 26-& (1969).

[63] Shiba, K., Diffusion Processes in Nuclear Materials, North Holland, Amsterdam, 1992.

[64] Bacmann, J.J., Cizeron, G.: Dorn Method in Study of Initial Phase of Uranium Dioxide Sintering. Journal of the American Ceramic Society, **51**, 209-212 (1968).

[65] Kutty, T.R.G., Khan, K.B., Hegde, P.V., Sengupta, A.K., Majumdar, S., Purushotham, D.S.C.: Densification behaviour and sintering kinetics Of PuO_2 pellets. Journal of Nuclear Materials, **297**, 120-128 (2001).

[66] Le Gall, R., Liao, G., Saindrenan, G.: In-situ SEM studies of grain boundary migration during recrystallization of cold-rolled nickel. Scripta Materialia, **41**, 427-432 (1999).

[67] Lens, A., Maurice, C., Driver, J.H.: Grain boundary mobilities during recrystallization of Al-Mn alloys as measured by in situ annealing experiments. Materials Science and Engineering a-Structural Materials Properties Microstructure and Processing, **403**, 144-153 (2005).

[68] Kurtz, S.K., Carpay, F.M.A.: Microstructure and Normal Grain-Growth in Metals and Ceramics .2. Experiment. Journal of Applied Physics, **51**, 5745-5754 (1980).

[69] Kurtz, S.K., Carpay, F.M.A.: Microstructure and Normal Grain-Growth in Metals and Ceramics .1. Theory. Journal of Applied Physics, **51**, 5725-5744 (1980).

[70] Wakai, F., Brakke, K.A.: Mechanics of sintering for coupled grain boundary and surface diffusion. Acta Materialia, **59**, 5379-5387 (2011).

[71] Podor, R., Clavier, N., Ravaux, J., Claparede, L., Dacheux, N., Bernache-Assollant, D.: Dynamic aspects of cerium dioxide sintering: HT-ESEM study of grain growth and pore elimination. Journal of the European Ceramic Society, **32**, 353-362 (2012).

[72] Hsueh, C.H., Evans, A.G.: Microstructure Evolution during Sintering - the Role of Evaporation Condensation. Acta Metallurgica, **31**, 189-198 (1983).

[73] Hsueh, C.H., Evans, A.G., Coble, R.L.: Microstructure Development during Final Intermediate Stage Sintering .1. Pore Grain-Boundary Separation. Acta Metallurgica, **30**, 1269-1279 (1982).

[74] Lange, F.F., Metcalf, M.: Processing-Related Fracture Origins .2. Agglomerate Motion and Cracklike Internal Surfaces Caused by Differential Sintering. Journal of the American Ceramic Society, **66**, 398-406 (1983).

[75] Nichols, F.A.: Kinetics of Diffusional Motion of Pores in Solids - a Review. Journal of Nuclear Materials, **30**, 143-& (1969).

[76] Bernard-Granger, G., Guizard, C.: Spark plasma sintering of a commercially available granulated zirconia powder: I. Sintering path and hypotheses about the mechanism(s) controlling densification. Acta Materialia, **55**, 3493-3504 (2007).

[77] Girard, E., Frittage du dioxyde d'uranium en présence d'hétérogénéités - Caractérisation de l'évolution microstructurale, PhD Thesis, Ecole Nationale des Mines de St-Etienne, 2004.

[78] Girard, E., Chaix, J.M., Valdivieso, F., Goeuriot, P., Léchelle, J.: Local study of defects during sintering of UO_2 : image processing and quantitative analysis tools. Image Analysis & Stereology, **27**, 79-85 (2008).

[79] Kelly, J.E.: Generation IV International Forum: A decade of progress through international cooperation. Progress in Nuclear Energy, (2014).

[80] Nkou Bouala, G.I., Clavier, N., Lechelle, J., Mesbah, A., Dacheux, N., Podor, R.: *In situ* HT-ESEM study of crystallites growth within CeO_2 microspheres. Ceramics International, **41**, 14703-14711 (2015).

[81] Scardi, P., Leoni, M., Mueller, M., Di Maggio, R.: In situ size-strain analysis of nanocrystalline ceria growth. Materials Science and Engineering A-Structural Materials Properties Microstructure and Processing, **528**, 77-82 (2010).

[82] Claparede, L., Clavier, N., Dacheux, N., Moisy, P., Podor, R., Ravaux, J.: Influence of Crystallization State and Microstructure on the Chemical Durability of Cerium-Neodymium Mixed Oxides. Inorganic Chemistry, **50**, 9059-9072 (2011).

[83] Nkou Bouala, G.I., Clavier, N., Léchelle, J., Monnier, J., Ricolleau, C., Dacheux, N., Podor, R.: High-temperature electron microscopy study of ThO_2 microspheres sintering. Journal of the European Ceramic Society, doi:10.1016/j.jeurceramsoc.2016.08.029 (2016).

[84] Coble, R.L.: Initial Sintering of Alumina and Hematite. Journal of the American Ceramic Society, **41**, 55-62 (1958).

[85] Nkou Bouala, G.I., Clavier, N., Martin, S., Lechelle, J., Favrichon, J., Brau, H.P., Dacheux, N., Podor, R.: From *in Situ* HT-ESEM Observations to Simulation: How Does Polycrystallinity Affects the Sintering of CeO_2 Microspheres? Journal of Physical Chemistry C, **120**, 386-395 (2016).

[86] Horlait, D., Claparede, L., Tocino, F., Clavier, N., Ravaux, J., Szenknect, S., Podor, R., Dacheux, N.: Environmental SEM monitoring of $Ce_{1-x}Ln_xO_{2-x/2}$ mixed-oxide microstructural evolution during dissolution. Journal of Materials Chemistry A, **2**, 5193-5203 (2014).